SPACE ENVIRONMENTS AND THEIR EFFECTS ON SPACE AUTOMATION AND ROBOTICS

by

Henry B. Garrett
The Jet Propulsion Laboratory
California Institute of Technology
4800 Oak Grove Dr.
Pasadena, CA, 91109

ABSTRACT

Automated and robotic systems will be exposed to a variety of environmental anomalies as a result of adverse interactions with the space environment. As an example, the coupling of electrical transients into control systems, due to EMI from plasma interactions and solar array arcing, may cause spurious commands that could be difficult to detect and correct in time to prevent damage during critical operations. Spacecraft glow and space debris could introduce false imaging information into optical sensor systems. The presentation provides a brief overview of the primary environments (plasma, neutral atmosphere, magnetic and electric fields, and solid particulates) that cause such adverse interactions. The descriptions, while brief, are intended to provide a basis for the other papers presented at this conference which detail the key interactions with automated and robotic systems. Given the growing complexity and sensitivity of automated and robotic space systems, an understanding of adverse space environments will be crucial to mitigating their effects.

INTRODUCTION

The space environment is far from benign in its effects on space systems. Automated and robotic systems, because of their complexity and autonomy, will in particular be threatened by environmental anomalies as a result of adverse interactions in space. The coupling of electrical transients into control systems, due, for example, to EMI resulting from plasma interactions and solar array arcing, may cause a variety of spurious commands that could be difficult to detect and correct in time to prevent damage during critical operations where human intervention might not be possible. As another example, spacecraft glow and space debris could introduce false imaging information into optical sensor systems causing guidance errors. This presentation will provide a brief overview of the more critical of these adverse environments (plasmas, neutral atmospheres, fields, and solid particulates) that could cause such interactions. Given the growing complexity and consequent sensitivity of automated and robotic space systems, an understanding of these environments and their interactions will be crucial to mitigating their effects.

ENVIRONMENTS

Introduction

In this review of the ambient space environment, 8 environments will be considered. The first, the neutral atmosphere, is primarily responsible for drag, glow, and oxygen erosion. The next 2 environments, the Earth's magnetic and electric fields, are responsible for magnetic torques and induced electric fields. The third electromagnetic environment to be discussed, the UV/EUV radiation environment, is not only responsible for the formation of the ionosphere but also for photoelectrons and long term changes in material properties. 4 plasma environments will be discussed: the Interplanetary Environment, the Plasmasphere/Ionosphere (responsible for ram/wake effects and solar array arcing), the Plasmasheet (the primary region for spacecraft charging) and it low altitude extension the Auroral Zone, and the Radiation Belts (the source environment for radiation dosage effects). Finally, the particulate environment, both man-made and meteoroid, will be briefly discussed. The intent is not to provide a detailed description of each of

these environments but rather to provide an overview of their chief characteristics as they apply to environmental interactions.

Neutral Atmosphere

By far the major environmental factor at shuttle altitudes is the earth's ambient neutral atmosphere. Whether it be through drag or the recently discovered interactions with atomic oxygen (glow and oxygen erosion), the effect of the neutral atmosphere (predominately the neutral atomic oxygen) on spacecraft dynamics and surfaces greatly exceeds any of the other effects that will be considered in this report. The 3 main sources of data at these low altitudes have been neutral mass spectrometers, accelerometers, and orbital drag calculations. Without going into detail, most models attempt to fit the observations with an algorithm that includes the exponential fall off of the neutral density, the effects of increasing solar activity (particularly in the ultraviolet), the local time, and geomagnetic activity. Of these, the large variations associated with increasing geomagnetic activity (and subsequent heating of the atmosphere) have eluded adequate modelling by this fitting process. Unfortunately, it is clear from many sources that these variations, particularly in density over the auroral zone, often dominate the neutral environment and that to date no adequate method of including these effects in the models has been devised (some recent very sophisticated theoretical computer models do hold promise, however). Here, some of the dominate features of the vertical and horizontal variations in density will be presented.

Consider first the vertical variations in the neutral atmosphere. In Fig. 1 (Carrigan and Skrivanek [1974]), the variations of the neutral atmosphere at orbital altitudes between about 100 km and 1000 km are plotted. This is, for example, the same region in which vehicle glow has been observed. For purposes of this review and for most practical applications, the neutral atmosphere can be considered according to Fig. 1 to consist mainly of atomic oxygen (note: atomic hydrogen can dominate occassionally above 500 km for low exospheric temperatures) with traces of molecular oxygen, molecular nitrogen, and atomic hydrogen over the altitude range of interest. Helium, nitric oxide, atomic nitrogen, and argon are also present below the one percent level (for general descriptions of the upper atmosphere, see Whitten and Poppoff [1971], Banks and Kockarts [1973] and references therein; widely used neutral atmosphere models are those of Jacchia [1972]; Jacchia [1977]; and Hedin [1987]). The thermal temperature of the constituents varies approximately exponentially from ~100 K at 100 km to 500-1500 K at 1000 km depending on solar cycle, latitude, and local time with excursions to 2000 K during high levels of geomagnetic activity. As spacecraft between 100 and 1000 km are moving at about 7.8 km/s, the resulting impact energy of the particles can reach values on the forward (or ram) surface of the spacecraft well in excess of 5 eV (varying from 4.6 eV for N to 10.25 eV for O2). These ram energies are sufficiently high to induce chemical reactions (including oxygen erosion). Further, the large ratio of the directed velocity to thermal velocity means that pronounced anisotropies exist in the flux to the vehicle. This has led to gross asymmetries in the glow phenomenon--surface glow appearing primarily on surfaces which face into the vehicle velocity vector.

2 types of models are often used to compute vertical profiles such as presented in Fig.1. These are the Jacchia family of models (i.e., Jacchia [1972], Jacchia [1972]) and the MSIS models (Hedin et al. [1977a]; Hedin et al. [1977b]; Hedin [1987]). These models are readily available in computer format and have been well developed over the last decade. For comparison, the more recent MSIS 1986 (Hedin [1987]) model and it companion, Jacchia 1977 (Jacchia [1977]), which are based on in-situ spacecraft measurements, deviate by about 20% from the older, drag based, Jacchia 1972 values on the average--a relatively small value given the much larger average uncertainties in the models themselves. These models, as illustrated in Figs. 2, 3, and 4 for the northern hemisphere and 400 km, can also be used to investigate horizontal variations in density, temperature, and composition. As can be seen, there is typically a two-fold increase in density from midnight to noon. Further, there is a pronounced shift by 2 hours of the peak in the density and temperature maxima away from local noon. This well know phenomena results from the rotation of the Earth and causes the peak in atmospheric heating to occur after local noon.

A typical shortcoming of the older, drag based models is that there are no clear density/temperature features associated with the auroral zone. This is directly due to the averaging techniques used in deriving models of this type which smooth out the density waves actually observed over the auroral zone--the more recent

MSIS 1986 and Jacchia 1977 do demonstrate auroral variations (these have been incorporated into a simple update of the Jacchia 1972 model by Slowey [1984]). An example of the variations at 120 km for the Jacchia substorm correction is presented in Fig. 5. Such correction factors, however, are only meaningful in an average sense--actual substorm variations can be an order of magnitude larger instanteously. Even so, the model results are useful in estimating the levels of atmospheric drag, shuttle "glow", and surface degradation.

Electromagnetic Environments

Magnetic and Electric Fields

Because of the rapid variations in the Earth's magnetosphere, the outer magnetic field beyond about 6 R_e is not precisely modelled. The approximate structure in the noon-midnight meridional plane is illustrated in Fig. 6 along with the major plasma regions that it delineates. In contrast, the geomagnetic field below 6 R_e and at Space Station/Shuttle altitudes is pretty accurately known. It can be crudely modelled, for example, in terms of a tilted (-11° from geographic north) magnetic dipole of magnitude 8×10^{25} G-cm3. Numerous, very accurate models of this field exist such as the International Geomagnetic Reference Field for 1985 (IGRF [1986]). As a typical example of these models, consider the somewhat simpler POGO magnetic field model (Knecht [1972]; Cain and Langel [1968]) which is the basis of the International Reference Ionosphere (IRI) and various radiation models. As is characteristic of most models of the near-Earth magnetic field, this model is a straight forward expansion of fits to the Earth's magnetic field in terms of spherical harmonics. As shown in Fig. 7 for 400 Km, the field varies in this model from a minimum of .25 G near the equator to .5 G over the polar caps. 2 peaks exist in the magnitude of the magnetic field (over the north pole, these are at 270°E and 90°E) and reflect the true complexity of the magnetic field in the auroral/polar cap regions (note: if vector components are considered, the maximum at 270° east longitude is the true "dip" magnetic pole). Likewise, there are two minima near the equator--the largest of these, the so-called South Atlantic Anomaly--will be important in our discussions of the radiation belts. Finally, it should be noted that geomagnetic storm variations are superimposed on this main field. These are typically less that .01 G so that even during a severe geomagnetic storm, magnetic fluctuations are small compared to the average field--a marked contrast with the atmospheric and ionospheric environments!

Besides magnetic torques (which are very system dependent), the earth's magnetic field can induce an electric field in a moving body by the vxB effect:

$$E = 0.1\ (vxB)\ V/m = .3\ V/m$$

at 400 Km

where:

v = spacecraft velocty = 7.6 km/s

B = .3 G

For the Shuttle, which is roughly 15 m x 24 m x 33m, potentials of 10 V could be induced by this effect. As systems grow to km or large dimensions, the induced fields will grow accordingly.

The induced electric field for a vehicle of 90° inclination are much more complicated than those for an equatorial orbit and, as would be anticipated, the largest electric fields are seen over the polar caps. Typical absolute values for a polar orbiting vehicle are presented in Fig. 8. In addition to these fields at polar latitudes, the ambient environment can also produce strong electric fields in the auroral regions. These fields can reach values of nearly 100 mV/m (Foster [1983])--a sizable fraction of the induced field. The fields are also comparable to the fields necessary to deflect charged particles in this environment as the particles have ambient energies of typically .1 eV (ram energies for the ions like oxygen can reach several eV, however) and thus must be taken into account when studying ionospheric fluxes.

UV/EUV (and X-Rays)

Solar ultraviolet (UV), extreme ultraviolet (EUV), and X-ray radiation are not only important to atmospheric and ionospheric dynamics but, through material surface changes and photoelectron emission, provide a major environmental factor for spacecraft at all altitudes. By UV/EUV radiation, we mean here the continuum and line spectrum between roughly 10 Å and 4000 Å. The energy in this spectral range is represented by a solar flux between 10^7 and 10^{10} photons/(cm^2 s) below 1000 Å. The flux rises

almost exponentially to 10^{16} photons/(cm^2 s) between 1000 Å and 10000 Å. The flux is not constant but varies in time due to a number of factors, one of which is the solar cycle variability. This radiation spectrum is also a complex variable of the atmospheric attenuation as a spacecraft moves in and out of the Earth's shadow (see Garrett and Forbes [1981]). An average spectrum is presented in Fig. 9 (Grard [1973]).

The shortest wavelengths, 10 Å-100 Å or less, are referred to as X-rays. This spectral range contributes to the ionization of the E-region. The spectral region from about 100 Å to 1000 Å, called EUV, is related to the photoionization processes of O_2, N_2, and O in the ionosphere and to thermospheric heating. UV radiation is the continuum and line spectrum between roughly 1000 Å and visible. This spectral region contributes to photo-dissociation, absorption, and scattering processes in the mesosphere, stratosphere, and troposphere. The spectral range from 10-1750 Å is absorbed in the lower thermosphere and effects the production of oxygen atoms and their vertical distribution above the mesopause. The Lyman-alpha line at 1216 Å plays a major role in the mesosphere through the disassociation of O_2, H_2O, and CO_2 and the ionization of nitric oxide. The spectral region between 1750 to 2400 Å leads to the dissociation of O_2 and to ozone production in the mesosphere and stratosphere. Between 2400 Å and 3300 Å, the solar irradiance is responsible for the disassociation of ozone and other trace gases that play a role in the stratospheric budget.

Plasma Environments

Introduction

There are 6 plasma regions with distinct characteristics that normally need to be considered in defining the Earth's magnetosphere or plasma environment. These are illustrated in Fig. 6. First there is the Solar Wind, a flowing magnetized plasma emitted by the Sun, that is responsible for shaping the Earth's magnetosphere. During severe geomagnetic activity, it has been observed within geosynchronous orbit but, typically is observed outside of about 10 R_e on the dayside. The region marking the transition between the Solar Wind and the Magnetosphere is called the Magnetosheath (we will not treat this region here but consider it as a subset of the Solar Wind for interactions purposes). Within the Magnetosphere, at low latitudes and altitudes, is the ionized extension of the Earth's atmosphere--the Ionosphere or, above 1000 km, the Plasmasphere. This cold plasma environment is typical of the Space Station environment. At higher latitudes and radial distance lies the Plasmasheet and its lower boundary, the Auroral Zone. This is the hot plasma primarily responsible for spacecraft charging. At still higher latitudes lies the Polar Cap environment. Normally this environment closely resembles the Ionosphere/Plasmasphere environment--only during solar flare or proton events, when energetic particles can gain direct access to the polar caps along magnetic field lines connected to the Solar Wind is this environment substantially different (here it will be considered a subset of the Ionospheric environment). Finally there is the very energetic Van Allen radiation belts that overlay the Plasmasphere and Plasmasheet. As these particles show significantly different time variations than the other two plasma environments, they will be treated as a separate population here.

Interplanetary Environment

Sun

The source of virtually all space disturbances is the Sun. Through a poorly understood process deep within the Sun, strong magnetic fields, thousands of times stronger than the Earth's magnetic field, are generated and brought to the solar surface. Material motions on or near the solar surface twist and shear these fields, ultimately producing instabilities in them. The fields in turn are responsible for the fundamental processes which affect space operations. Although the visible surface of the Sun is at a temperature of abut 6000 K, the magnetic fields serve as a conduit channelling energy into the outer solar atmosphere. This outer atmosphere, the solar corona visible during a solar eclipse or directly observable from space, is thereby heated to temperatures over 10^6 K. At this high temperature the solar corona "boils" off into space at velocities of about 500 km/s, carrying some of the imbedded magnetic field with it. This "solar wind" is highly time variant with a complex magnetic structure. When the solar wind interacts with the Earth's own magnetic field some three to five days after it left the Sun, space environmental problems are born.

A far more energetic process, and potentially damaging situation, occurs when very strong magnetic fields in the solar corona reach a critical

instability. On times scales of seconds the strong fields are unstable enough to "snap" thereby adjusting and relaxing to remove the instability. A considerable amount of energy, up to .1% of the total solar enery output or about 10^{32} ergs, is released during this "flare". A solar flare typically lasts from a few minutes to a few hours and heats the surrounding corona to temperatures in excess of $2x10^7$ K. Associated with the heating, large fluxes of atomic particles, electrons, neutrons, and protons, are accelerated and expelled from the Sun. There are also substantial radio bursts and X-ray emissions. The X-ray emissions and radio bursts arrive at the Earth in 8 minutes and are the first evidence at the Earth that a solar flare has occured. About an hour later the highest energy particles, mostly neutrons, protons, and heavier atomic nuclei, arrive. However it is the flare blast wave or solar wind shock, consisting of charged particles (electrons), and carrying with it portions of the tangled coronal magnetic field, arriving several days later at the Earth which represents the most serious hazard for space systems in Earth orbit (as opposed to systems in interplanetary space where single event upsets due to the solar flare protons are the most serious problem) as this shock can initiate a major geomagnetic storm and can lead to pronounced enhancements of the radiation belts.

The Sun has a roughly periodic activity cycle. Due to poorly understood phenomena deep within the solar interior, solar magnetic field penetration and eruption through the solar surface has an eleven year cycle. Although the solar wind is fairly constant during this cycle, solar flare related phenomena occur far more frequently during solar maximum (in terms of sunspot number). The current solar cycle, which is particularly severe, is expected to peak in early 1990. There is some evidence that changes in overall solar energy output of up to 1% are also associated with the solar cycle. These variations are enough to affect global terrestrial weather patterns. The solar cycles themselves, while fairly predictable in time, have peak activity levels which may vary by factors of four from one maximum to the next (Fig. 10). Moreover, historical records have indicated relatively long periods, for example, during most of the 18th century, when there were no discernable solar cycles. It is, however, the effects of solar flares and geomagnetic storms that most impact the Space Station and Shuttle environments. Although solar flares are far less frequent during solar minimum, flare related effects can be greater in the terrestrial magnetosphere because the interplanetary fields, through which the flare material must travel, are less complicated and solar flare particles can more easily gain access to the earth's polar caps. Geomagnetic activity at the Earth also shows this variation. Although the number of geomagnetic storms goes down during minimums in solar activity, the level of a given storm, even during the lowest levels of solar activity, can be among the highest ever seen.

Solar Wind

The dominate environment in the Solar System is that of the solar atmosphere or heliosphere--the Solar Wind--and, while it does not directly contribute to Shuttle and Space Station interactions, it the primary energy source of geomagnetic activity which does. As discussed, the Solar Wind is the low density plasma (predominately hydrogen ions with some helium) that is being continuously emitted from the solar corona at supersonic speeds. The plasma is characterized by a residual magnetic field (typically a few 10's of nT; 1 nT= 1 nano Tesla or 1 gamma) and variable velocity and density. The Solar Wind velocity vector is observed to be dominantly in a radial direction in the ecliptic plane with a magnitude of 200 to 500 km/s. Since the Sun rotates with a period of 27 days, the Solar Wind takes on a spiral structure with the spirals marked by regions of similar magnetic polarity (Fig. 11). At present, based on in-situ measurements from the Pioneer spacecraft, we know that this environment extends out to and beyond the orbits of Pluto and Neptune where at some point it terminates in the interstellar medium. Typical plasma values for the Solar Wind are for distances corresponding to near Mercury 50 cm^{-3} and 50 eV, 2 cm^{-3} and 10 eV for the ions and 50 eV for the electrons at the Earth, and .2 cm^{-3} and 1 eV for the ions and 10 eV at Jupiter. The Solar Wind represented by these values can be a significant source of spacecraft charging in the interplanetary medium. Finally, it should be noted that it is now accepted that there is a direct relationship betweent the direction of the Solar Wind magnetic field and geomagnetic activity--when the Solar Wind field points southward, the likelihood of geomagnetic activity is greatly enhanced. The reason for this connection is not completely understood but is generally believed to be due to increased coupling and energy transfer between the Solar Wind magnetic field and the Earth's geomagnetic field.

Plasmasphere/Ionosphere

Illustrated in Figs. 12 and 13 (Carrigan and Skrivanek [1974]) are various vertical profiles of the ionosphere. On the sunlit hemisphere of the Earth, X-rays, EUV, and UV radiation penetrate the neutral atmosphere, ionizing and exciting the molecules present. As the radiation penetrates, there is a balance between increasing neutral density and increasing absorption that leads to the formation of ionized layers (principally the F layer between 150 and 1000 km, the E layer between 100 and 150 km, and the D layer between 60 and 100 km) that gives rise to the mean structure called the ionosphere (for general descriptions of the upper ionosphere, see Whitten and Poppoff [1971], Banks and Kockarts [1973] and references therein; a widely used ionospheric model is the International Reference Ionosphere--IRI-86; Rawer and Bradley [1987]). These layers are the combined result of the absorption/increasing-density process and complex chemical reactions within the atmosphere and ionosphere. As illustrated by the horizontal profiles in Fig. 14 from the IRI model, the local time peak in the ionospheric density parallels that of the neutral density bulge--occurring approximately 2 hours after local noon. The ionospheric composition likewise follows that of the neutral atmosphere, varying roughly from NO^+/O_2^+-dominated in the D region, to O^+-dominated in the E region, to H^+-dominated in the F region (chemical reactions complicate the picture). Densities reach 10^6 cm^{-3} at the peak in the F region at about 300 km on the sunlit side. At night, the peak ion density can fall below 10^5 cm^{-3} and the composition change from O^+ to H^+ above 500 km. Temperatures follow roughly that of the neutral atmosphere--increasing exponentially from a few 100 K at 50-60 km to 2000-3000 K above 500 km (i.e., a few tenths of an eV). The electron temperature tends to be a factor of two greater than that of the neutrals, with the ion temperature falling in between.

In order to systematically evaluate the effects of the ionosphere on automated and robotic systems, fairly detailed models of the Space Station environment are required. At present relatively few ionospheric models are available and most of these only predict electron densities--the most readily measureable quantity by ground means and the most important to radio propagation. Unfortunately, the ionospheric composition is particularly critical to adequate modelling of the Space Station ram/wake. The principle ionospheric model currently in use is the International Reference Ionosphere (Rawer and Bradley [1987]). This computer model, based primarily on ground based observations of the total electron content, is the only readily available computer model that gives both the electron and ion composition and temperature as a function of longitude, latitude, altitude (65 to 1000 km), solar activity (by means of the sunspot number, R), and time (year and local). Although the model is limited (it is confined to R values of 100 or less whereas R values of 200 may occur during solar maximum), it is the "best" available comprehensive model of the ionosphere. As an example of the output, the model predicts that, unlike the neutral temperature, the electron temperature increases by a factor of 2 in going from the equator to the pole (Fig. 14). The IRI computer simulation of the ionosphere shows a complex local time variation with the peak in electron density on the day side and/or in the auroral zones. These variations in turn lead to pronounced variations in the ram/wake structure of the Space Station that can cause interactions with systems operating in and near the Space Station or a similar large structure.

A major shortcoming of current ionopheric (and atmospheric models also) is their inability to properly model high latitude geomagnetic effects. As will be discussed, above about 60° geomagnetic latitude, the Earth is subjected to intense fluxes of high energy electrons and ions from the magnetosphere of the Earth and by direct entry of solar flare particles. These particles (typical energies between 100 eV and 10 KeV) generate considerable ionization that can easily excede the UV/EUV levels at these latitudes below 1000 km. Unlike the fairly constant UV/EUV fluxes, these corpuscular precipitation events (as they are some times called) can vary greatly in time--often occurring in less than a 1/2 hour. They are intimately associated with the auroral displays that are seen in the polar regions and indeed they are the cause. The ionization can increase orders of magnitude in a similar short time period adding great complexity to the polar ionosphere. Currently, only a few very complex "Thermosphere General Circulation Models" (TGCMs) can adequately model these effects. As yet it very hard to apply the results of these models to practical examples as the results are too complex to readily interpret.

Aurora/Plasma Sheet

The flow of the magnetized Solar Wind plasma past the Earth's magnetic field creates a long (perhaps 1000's of R_e in length) magnetic cavity in the antisunward direction (see Fig. 6). Inside this cavity, extending roughly from about geosynchronous orbit to the magnetopause in the sunward direction and from geosychronous along the length of the magnetic tail in the antisunward direction, is a thick "sheet" of warm plasma. This plasma sheet, as it is called, is believed to extend earthward from geosynchronous orbit along the magnetic field lines that map into the auroral zones in the northern and southern hemispheres (roughly between 55° and 75° depending on geomagnetic activity). The "temperature" of the plasma ranges between 100's of eV to 10's of keV for the electrons and 1000's of eV to 10's of keV for the ions (primarily hydrogen ions with variable concentrations of oxygen ions). The density is quite variable, changing from less than 1 to 10's of particles per cubic centimeter in minutes or less. The spatial location of the inner plasma sheet boundary is roughly between 5 and 8 R_e--varying greatly with geomagnetic activity and spatial location. The plasma sheet is marked by rapid temporal fluctuations called geomagnetic substorms (or, more precisely, "injection events") which compress it inward in the equatorial plane and increase its density and to a lesser extent its average energy. These events have been found to correlate with sharp increases in surface charging on geosynchronous spacecraft and represent the major source of surface charging within the Solar System. The events are believed to manifest themselves as aurora at lower altitudes--the plasma sheet serves as a giant electron beam source which paints the Earth's upper atmosphere which then acts like an oscilliscope screen, the aurora being the "trace". It is indeed these high latitude aurora which pose the greatest threat to low altitude, polar orbiting systems. A typical spectrum is presented in Fig. 15 (Gussenhoven et al. [1985]).

The most dramatic changes in the Earth's environment at Space Station altitudes are brought about by geomagnetic substorms. These changes are reflected in visible auroral displays and in intense particle and field variations in the auroral regions down to 100 km. The precipitating particle patterns (chiefly electrons as the ions are typically scattered high in the atmosphere by various processes) can be roughly divided into a broad, diffuse background and discrete features. Simple auroral flux models (Hardy et al. [1985] and Fuller-Rowell and Evans [1987]) of the diffuse populations are available. They predict a .1-1 keV particle population flowing down along magnetic field lines into the upper atmosphere. The pattern can be approximated by a simple sinusoidal variation in geomagnetic local time, a gaussian in latitude (the peak occurring near 65°-75°), and a roughly linear increase in the geomagnetic Kp index. Superimposed on this are the so-called discrete aurora characterized by latitudionally narrow features (some believed to be smaller than a km) and great longitudional extent (10's of degrees). The particles, again primarily electrons, have energies in the 1 keV to 10 keV range. Even though the flux of these particles can reach 10's of nA, the ambient flux due to the cold plasma running into the Shuttle approaches mA. Only above about 700 km, and then rarely, can the auroral fluxes excede the ionospheric density. It is, however, in the wake of the Shuttle or other large structure as it passes through the aurora that problems can occur. In the wake, as the ambient ionospheric ions can not penetrate effectively (the cold ions, primarily O^+, have thermal velocities of only 2-3 km/s whereas the orbital velocity at Space Station altitudes is on the order of 7 km/s) and keep the cold electrons out, only the high energy electrons associated with the aurora can penetrate. They thus determine the potential of electrically isolated surfaces in the wake.

Radiation

Introduction

The high energy radiation environment will be assumed here to consist of electrons with energies greater than 100 KeV and protons with energies greater than 1 MeV but with energies below 1 BeV. Above about 500 MeV energy, the particles are typically considered solar flare particles or Cosmic Rays--these will be considered separately. Heavy ions associated with solar flares will also be briefly mentioned. It should also be noted that there is increasing evidence that heavy ions, particularly O^+, are common if not dominant components of the Earth's radiation belts, but the measurements are still being evaluated. Currently, this radiation regime is defined in terms of two sets of models--the National Space Science Data Center (NSSDC) AE and AP models (these are further divided into versions at Solar Maximum--AE8MAX and APMAX--and Solar Minimum--AE8MIN and AP8MIN). Therefore, rather than complicate the definition of this environment with a discussion of the many variations typical of the regime, we will, following a description of the form of the AE/AP models, define the radiation environment in terms of them.

Trapped Particles

There are potentially many different ways to model the Earth's radiation environment. Fortunately, the use of adiabatic invariants, the introduction of the McIlwain's B-L coordinates, and the predominance of the AE/AP series of radiation models have produced a uniform set of practical models. For the purpose of studying radiation effects on long duration space missions, these AE/AP models produced by the NSSDC have proven to be very useful. Here the major characteristics of the radiation environment will be summarized in terms of these AE/AP type of models. It should be remembered, however, that there are other means of representing the environment that may be more appropriate for specific uses. The AE/AP models assume that the flux of particles can be given as a function of B and L coordinates integrated over some energy interval. Units are typically "particles per square centimeter per second" with the integrated energy channel being from the stated energy (typically 40 keV to 4 MeV for electrons in the AE electron models and 1 to 400 MeV for the AP proton models). A valuable attribute of these models is that, in principle, it is possible to construct this type of simple model by one measurement of the fluxes at all pitch angles as a satellite moves away from the Earth in the magnetic equatorial plane. As modelling of the Earth's radiation environment is a complex process at best, the AE/AP do have some limitations--for example, the effects of inadequate data coverage and the lack of recent data. The NSSDC has recently issued the AE8/AP8 versions of the model which correct some of these inadequacies.

The major difficulty in developing a model of the Earth's radiation belts is that both space and time must be factored into the model. Although the use of the adiabatic invariants and B-L coordinates are very useful in simplifying this task, in reality asymmetries in the Earth's magnetic and electric fields and their time variations introduce significant complications into the modelling process. In particular, due to such effects as "shell-splitting" (particles of the same energy but different pitch angles tend to follow slightly different drift paths around the Earth so that particles observed together at the equator on one side of the Earth are separated in radial distance on the other side), distortions in the Earth's magnetosphere, and similar effects force the inclusion of time and local-time (or, less precisely, longitudional) variables. The AE/AP model fluxes, for example, can be parametrically represented by:

$$J(>E,B,L,\theta,T) = N(>E,L)\Phi(>E,L,\theta)G(B,L)$$

where J is the integral omnidirectional flux, >E means for all energies above E, θ is the local time, and T is the epoch (or date). Data from many different satellites are averaged in discrete B and L bins to determine the B-L variation G, in energy, L, and local time to determine the local time variation Φ (note: B variations were ignored because there was often too little data to allow simultaneous binning in terms of B also), and in energy and L bins to determine the energy variations N.

Fig. 16 for 1 MeV electrons and 10 MeV protons from the AE8 and AP8 models respectively illustrates the basic structure of the radiation belts. In particular, the electron contours show a dual peak (the protons have a similar structure but the division between the peaks is less obvious). Typically, therefore, the radiation belts are divided into "inner-zone" and "outer-zone" populations. This division also roughly corresponds, for the electrons, to an inner belt which is weakly affected by geomagnetic storms and an outer belt which is greatly affected by storms. The L-shell region up to L~2.5 is termed the inner-zone while the region beyond L~3 is considered to be the outer-zone with a "slot" region of reduced density in between. The inner-zone electrons peak around L = 1.45 to 1.5 (typical values at 1.45 are: $>10^8$ for $E\geq0.1$ MeV; $>10^6$ for $E\geq1$ MeV; $>10^5$ for $E\geq2$ MeV; integral, omnidirectional flux in units of $cm^{-2}\ s^{-1}$). Little variation with geomagnetic activity is seen below L~1.6. The inner-zone protons are very stable, varying inversely with atmospheric density (the fluxes are lower at solar maximum when the atmospheric density is highest). The proton flux peaks near L = 1.45 (typical values at 1.45 are: $>10^4$ for $E\geq100$ MeV and $>10^3$ at 300 MeV). In the outer zone, the peak L shell varies with energy for the electrons (typical values are: $>10^8$ for $E\geq0.1$ MeV, L = 6; $>10^7$ for $E\geq1$ MeV, L = 5; $>10^5$ for $E\geq4$ MeV, L = 4; units are as above). Flux increases can be as great as 10^3 in less than a day during a geomagnetic storm. The outer-zone protons do not show as strong a division into an outer belt as the electrons nor as much variation with geomagnetic activity. Protons with $E\geq1$ MeV peak at about L = 3 while protons with $E\geq10$ MeV peak at about L = 2.5 (typical intensities are: $>10^8$ for $E\geq0.1$ MeV; $>10^7$ for $E\geq1$ MeV; $>10^5$ for $E\geq10$ MeV; $<10^2$ for $E\geq100$ MeV; units as above). (Note: all numbers are adapated from Vampola [1989].)

Galactic Cosmic Rays and Solar Flares

The AE/AP models only describe the trapped electron and proton environments. Recently, with increasing concern over single event upsets, there has been a need for models of the high energy, high charge number ions above hydrogen in mass that are primarily associated with solar flares. These particles, generally associated with solar flare proton events and Galactic Cosmic Rays, can cause bit flips in sensitive electronic components without damaging the components. These logic changes can seriously affect a satellite's control systems if permitted to go uncorrected. As yet, models capable of accurately predicting the occurrence frequency of solar flares are not reliable. Recent models by Feynman et al. [1989] of solar flare proton events, however, hold the key to future progress in this area. Here, instead, the physical characteristics of the events will be presented.

Consider first Galactic Cosmic Rays. Galactic Cosmic Rays (GCR) are primarily interplanetary protons and ionized heavy nuclei with energies from ~1 MeV/nucleon to higher than $\sim 10^{10}$ GeV/nucleon. Electrons are also a constituent of GCR, but their measured intensities at energies above ~100 MeV are at least 1 order of magnitude smaller than that of the protons and are usually ignored. Experimental studies indicate that cosmic ray fluxes are isotropic over the entire energy range, suggesting that they are galactic and/or extragalactic in origin. Figs. 17 and 18 display the observed cosmic ray energy spectrum and abundance distribution for the chemical elements in the energy range of ~100 MeV/nucleon to ~1 GeV/nucleon from hydrogen to the iron group (Meyer et al. [1974]). For comparison, solar system abundances are also shown in the figure. Note that the two abundance distributions are strikingly similar.

In addition to Galactic Cosmic Rays, hydrogen and heavy nuclei in the ~1 MeV/nucleon to ~10 GeV/nucleon energy range are ejected during a solar flare. Their intensities are generally a few to several orders of magnitude larger than those of Galactic Cosmic Rays at these lower energies, depending on the size of solar flare. Detailed studies of solar flares are limited by a current lack of sufficient data, particularly that of the relative elemental abundances, and their unpredictable occurrence frequency. Solar flare particles (Galactic Cosmic Rays also, but their fluences are typically too low to be of concern), because of their high penetrating abilities and ionizing powers, are known to induce single event upsets (SEU) and other malfunctions in digital microelectronics devices even at Space Station altitudes. A series of reports by J. Adams and his collaborators at Naval Research Laboratory (NRL) provide the relevant formulations and information on this important subject (Adams et al. [1981]; Adams et al. [1983]; Tsao et al. [1984]; Adams et al. [1986]). In these reports, in addition to the Galactic Cosmic Ray model, a worst-case solar flare model is developed based on the combined features of the two largest solar flares ever observed (one in 1956 and one in 1972). A comparison between the galactic cosmic ray flux and the worst-case solar flare proton event in 1972 is presented in Fig. 19. As shown, the worst-case solar flare proton flux is ~5 orders of magnitude larger than the galactic cosmic ray flux, but becomes "softer" above ~10 GeV.

In evaluating the effects of Galactic Cosmic Rays and solar flare particles on spacecraft, one final point needs to be considered. That is, for the low Earth orbit environment, the geomagnetic field provides shielding against incident Galactic Cosmic Rays and solar flare particles as it can effectively deflect (through the Lorentz force) the lower energy cosmic ray and solar flare particles. Because of the approximate dipole nature of the geomagnetic field, vertical particle velocities in the polar regions are essentially parallel to the magnetic field resulting in almost vanishing Lorentz force so that the particles can gain direct access. At low inclinations, only particles with sufficiently high energy, or "rigidity", can penetrate through the magnetic shielding.

Particulates

Introduction

Although the primary effect of the ambient, macroscopic particulate environment represented by space debris and interplanetary meteoroids is mechanical (i.e., impact craters), it can also indirectly change the EM characteristics of spacecraft systems in several ways. For instance, penetration of insulation can result in "pinholes" that expose the underlying conductors to the plasma environment. The subsequent current collection and related effects may seriously alter the local surface fields. The ejecta cloud produced by an impact can be partially ionized, causing charging and/or an electromagnetic pulse. Also,

cumulative erosion effects will eventually result in failure of exposed insulation, solar array surfaces, and wiring. The sources of these particulates in Earth orbit are both extraterrestrial--comets--and terrestrial--waste products and the remains of previous satellites. Given that the manmade debris is already pervasive in low Earth orbit, it will be considered as part of the "natural", or pre-existing, environment. Each of these particulate environments will be separately considered.

Interplanetary Meteoroid Environment

The close of the decade of the 60's saw the completion of three definitive NASA design criteria documents on the meteoroid environment and its effects on spacecraft systems. As of this date, the models presented in those documents still represent the official NASA meteoroid environment despite more recent data on the in-situ environment. The three documents are:

1.) "NASA Space Vehicle Design Criteria (Environment); Meteoroid Environment Model (Near Earth to Lunar Surface)", NASA SP-8013 [1969].

2.) "NASA Space Vehicle Design Criteria (Environment); Meteoroid environment Model (Interplanetary and Planetary)", NASA SP-8038 [1970].

3.) "NASA Space Vehicle Design Criteria (Structures); Meteoroid Damage Assessment", NASA SP-8042 [1970].

The first document defines the meteoroid environment between the Earth's surface and the Moon and is the primary model used for the interplanetary meteoroid flux. It provides working definitions of the three principle quantities needed to define the meteoroid environment: their mass versus number density, their velocity distribution, and their composition. Included in the document are listings of interplanetary meteor streams and the Earth-based meteor observations on which the models are based. The second document presents an extrapolation of the Earth-based observations to interplanetary space for meteoroids of both cometary and asteroidal origin. The final document outlines ground studies of high velocity impacts, methods of modeling meteoroid penetration, and techniques for limiting meteoroid damage. Of the three documents, the first is the primary sources of the material to be presented here and will be discussed in more detail.

Meteoroids as defined by the NASA documents are solid particles orbiting in space that are either of cometary or asteroidal origin. The spatial volume of interest ranges from 0.1 to 30.0 astronomical units (AU). The mass range is from 10^{-12} to 10^{22} g. Knowledge of these particles is based primarily on Earth-based observations of meteors, comets, asteroids, the zodiacal light, and in-situ rocket and spacecraft measurements. In all cases, the flux versus mass of the particles, the basic quantity required to model the meteoroid environment, is not directly measured but must be inferred (e.g., from light intensity, crater distributions, etc.). The ground-based measurements consist principally of photographic and radar observations. These yield fluxes for masses from 10^{-3} g or larger and 10^{-6} to 10^{-2} g respectively. Observations of the zodiacal light and direct in-situ measurements cover a much smaller mass--typically 10^{-13} to 10^{-6} g. At the other extreme, telescopic observations of asteroids and planetary and lunar crater counts are used to determine the distribution from 50 km and up. As should be obvious, there are large data gaps in the assumed distribution. Of most concern to the Space Station is the range from about 10^{-3} to 10 g as these particles pose the major threat of catastrophic failure to crew modules. Of more concern for pinholes, the major problem for EMC, is the mass range from 10^{-3} down to 10^{-9} g as these particles will have sufficient flux to erode surfaces and sufficient energy to penetrate protective coatings. Meteorites fall in this range but due to the infrequency of actual observed impacts and the difficulty of relating the final mass to the original mass, little data are available. Sufficient information does exist to justify dividing the observations into two groups: those of cometary origin (average density around 0.5 g-cm^{-3}) and those of asteroidal origin (average density around 3.5 g-cm^{-3}), however, it is the cometary meteoroids which predominate near Earth.

Cometary Meteoroids

Cometary meteoroids in the mass range of interest (<10 g) are believed to be the solid remains of large water-ice comets that have long since evaporated or broken up due to collisions. The remaining silicate or chondritic material is of very low density (0.16 to 4 g-cm^{-3}) with an assumed value of 0.5 g-cm^{-3} for the NASA model. The primary flux of meteoroids inside 1.5 AU is made up of these cometary meteoroids as the denser asteroidal meteoroids are concentrated in the asteroid belts and peak at 2.5 AU. The

cometary integral mass distribution, derived from the observations discussed previously and assumed in the NASA Cometary Model, is plotted in Fig. 20. The velocity distribution relative to a massless Earth is presented in Fig. 21 for several different models (Morgan et al. [1988]) with the equivalent NASA model results plotted as a solid line ("massless Earth" means that the data have been corrected for the gravitational pull of the Earth).

NASA 8013 describes the total cometary meteor flux at Earth by the following:

$$\log_{10} F_c = -14.37 - 1.213 \log_{10} m$$

for $10^{-6} \leq m \leq 1$

$$\log_{10} F_c = -14.339 - 1.584 \log_{10}^2 m - .063 (\log_{10}^2 m)$$

for $10^{-12} \leq m \leq 10^{-6}$

where F_c is the number of cometary meteoroid impacts of mass m grams or larger per square meter per second. The gravitationally focused, unshielded flux, F_c, must be multiplied by a defocusing factor for Earth, G_E, as well as a shielding factor, ϵ.

The defocusing factor which corrects for the gravitational enhancement at a given distance from the Earth's center may be expressed as:

$$G_E = 0.568 + 0.432 (R_e/r)$$

The correction due to the physical presence of the Earth itself, which shields the spacecraft (randomly oriented) is expressed as:

$$\epsilon = 0.5 + 0.5 (1 - (R_e/r))^{.5}$$

Multiplying by eta has the effect of subtracting out the flux within the solid angle subtended by the shielding body.

where:

R_e = the Earth's radius
r = the distance of the spacecraft from the center of the Earth

Space Debris

Increasing spaceflight operations in the Earth's vicinity have led to the creation of an artificial shell of debris around the Earth. This shell of debris poses an impact threat greater than the natural meteoroid environment within 2000 km of the Earth's surface. The Earth debris impact threat is credible and requires careful consideration. It is the purpose of this section to briefly review the basis of the existing debris model for spacecraft in low Earth orbit and to illustrate how debris impact calculations are carried out.

The main sources of orbital debris are orbiting spacecraft, fragments from exploded boosters or spacecraft, metal oxides and particulates from solid rocket motors, and ejected items from previous missions. These in turn collide with each other creating further debris--the Shuttle Challenger had one of its windows pitted by a debris particle, clearly illustrating the reality of such collisions. There are currently several sets of observational data for this growing threat. First, there are ground based optical and radar observations that form the bulk of the information. These are primarily from the US Space Command orbital element sets for objects of 10 cm diameter and larger, from optical measurements by MIT for objects 2 cm in diameter and larger, and from debris particle albedo measurements using an IR telescope at ATMOS/MOTIF, US Space Command radars, and NASA and Space Command telescopes. Second, for particles between 10^{-6} and 10^{-3} cm in diameter, in-situ measurements are available from sample surfaces retrieved from the Solar Maximum Mission (Laurance and Brownlee [1986]) at 500 km altitude. The NASA model and these observations are compared as a function of height in Fig. 22. Data from IRAS and other in-situ experiments are expected to further expand the debris data base in the near future.

Kessler (Kessler et al. [1989]) estimates the cumulative flux of debris on orbiting spacecraft to be given by:

$$F(d,h,i,t,S) = k \Phi(h,S) \Psi(i) (F_1(d) g_1(t) + F_2(d) g_2(d))$$

where:

F = Flux in impacts per square meter of surface area per year
k = 1 for a randomly tumbling surface; must be calculated for a directional surface
d = Debris diameter (cm)
t = Time (years)
h = Altitude (km); h < 2000 km
S = 13-month smoothed 10.7 cm wavelength solar flux (10^4 Jy); retarded by 1 year from t
i = Inclination (degrees)

and

$$\Phi(h,S) = \Phi_1(h,S)/(\Phi_1(h,S) + 1)$$

$$\Phi_1(h,S) = 10^{(h/200 - S/140 - 1.5)}$$

$$F_1(d) = 1.05 \times 10^{-5}\, d^{-2.5}$$

$$F_2(d) = 7 \times 10^{10}\, (d + 700)^{-6}$$

$$g_1(t) = (1 + 2p)^{(t-1985)}$$

$$g_2(t) = (1 + p)^{(t-1985)}$$

p = Annual growth rate of mass in orbit = 0.05

Fig. 20 (Kessler et al. [1989]) compares the debris flux predicted by this model and the NASA SP-8013 [1969] meteoroid flux at an altitude of 500 km.

CONCLUSION

This paper has reviewed the key ambient environments that could potentially cause operational anomalies or damage to automated and robotic systems. These environments cover large portions of the electromagnetic and kinetic energy spectrum. As a result, these environments are difficult to protect against and will require mitigation techniques. In many situations, these protection methods have yet to be determined. Ultimately, the information presented here will be critical to the developmemnt of these methods. Hopefully, this review will prove to be a userful starting point in this process.

"The research described in this paper was carried out by the Jet Propulsion Laboratory, California Institute of Technology, under a contract with the National Aeronautics and Space Administration."

REFERENCES

Adams, J.H., Jr., R. Silberberg, and C.H. Tsao, "Cosmic Ray Effects on Microelectronics, Part I: The Near-Earth Particle Environment", NRL Memorandum Report 4506, Naval Research Laboratory, Washington, DC 20375, 1981.

Adams, J.H., Jr., J.R. Letaw, and D.F. Smart, "Cosmic Ray Effects on Microelectronics, Part II: The Geomagnetic Cutoff", NRL Memorandum Report 5099, Naval Research Laboratory, Washington, DC 20375, 1983.

Adams, J.H., Jr., "Cosmic Ray Effects on Microelectronics, Part IV", NRL Memorandum Report 5901, Naval Research Laboratory, Washington, DC 20375, 1986.

Banks, P.M., and G. Kockarts, "Aeronomy, Parts A and B", Academic Press, New York, 1973.

Cain, J.C., and R.A. Langel, "The Geomagnetic Survey by the Polar Orbiting Geophysical Observatories Ogo-2 and Ogo-4, 1965-1967", GSFC REP X-613-68-502, Greenbelt, MD, 1968.

Carrigan, A.L., and R.A. Skrivanek, "The Aerospace Environment", AFCRL Chart, 1974.

Daly, E.J., "The Evaluation of Space Radiation Environments for ESA Projects", ESA Journal, 12, 229-247, 1988.

Feynman, J., T. Armstrong, L. Dao-Gibner, and S. Silverman, "A New Interplanetary Proton Fluence Model", to appear in J. SPACECRAFT, 1989.

Foster, J.C., "An Empirical Electric Field Model Derived from Chatanika Radar Data", J. GEOPHYS. RES., 88, 981-987, 1983,

Fuller-Rowell, T.J., and D.S. Evans, "Height-Integrated Pedersen and Hall Conductivity Patterns Inferred From the TIROS-NOAA Satellite Data", J. GEOPHYS. RES., 92, 7606-7618, 1987.

Garrett, H.B., and Forbes, J.M., "A Model of Solar Flux Attenuation During Eclipse Passage and Its Effects on Photoelectron Emission from Satellite Surfaces", Planet. Space Sci., 29, pp. 601-607, 1981.

Grard, R.J.L., "Properties of the Satellite Photoelectron Sheath Derived from Photoemission Laboratory Measurements", J. Geophys. Res., 78, pp. 2885-2906, 1973b.

Gussenhoven, M.S., D.A. Hardy, F. Rich, W.J. Burke, and H.-C. Yeh, "High Level Spacecraft Charging in the Low Altitude Polar Environment", J. GEOPHYS. RES., 90, 11009, 1985.

Hardy, D.A., and M.S. Gussenhoven, "A Statistical Model of Auroral Electron Precipitation", J. GEOPHYS. RES, 90, 4229-4248, 1985.

Hedin, A.E., Jr., J.E. Salah, J.V. Evans, C.A. Reber, G.P. Newton, N.W. Spencer, D.C. Kayser, D. Alcayde, P. Bauer, L. Cogger, and J.P. McClure, "A Global Thermospheric Model based on Mass Spectrometer and Incoherent Scatter Data, MSIS 1, N2 Density and Temperature", J. GEOPHYS. RES., 82, 2139-2147, 1977a.

Hedin, A.E., Jr., C.A. Reber, G.P. Newton, N.W. Spencer, H.C. Brinton, H.G. Mayr, and W.E. Potter, "A Global Thermospheric Model based on Mass Spectrometer and Incoherent Scatter Data, MSIS 2, Composition", J. GEOPHYS. RES., 82, 2148-2156, 1977b.

Hedin, A.E., "MSIS-86 Thermospheric Model", J. GEOPHYS. RES., 92, pp. 4649-4662, 1987.

IGRF, "International Geomagnetic Reference Field Revision 1985", EOS, 523-524, 17 June, 1986.

Jacchia, L.G., "Atmospheric Models in the Region from 110 to 2000 km", in CIRA 1972, Akademie-Verlag, Berlin, pp. 225-328, 1972.

Jacchia, L.G., "Thermospheric Temperature, Density, and Composition: New Models", Spec. Rep., 375, Smithson. Astrophys. Observ., Cambridge, Mass., 1977.

Kessler, D.J., R.C. Reynolds, and P.D. Anz-Meador, "Orbital Debris Environment for Spacecraft Designed to Operate in Low Earth Orbit", NASA TM-100-471, 1989.

Knecht, D.J., "The Geomagnetic Field", Air Force Surveys in Geophysics, No. 246, AFCRL-72-0570, 26 Sept., 1972.

Laurance, M.R., and Brownlee, D.E., "The Flux of Meteoroids and Orbital Space Debris Striking Satellites in Low Earth Orbit", NATURE, 323, pp. 136-138, 1986.

Meyer, P., R. Ramaty, and R. Webber, "Cosmic Rays - Astronomy with Energetic Particles", PHYSICS TODAY, Oct., 1974.

Morgan, T.H., Zook, H.A., and Potter, A.E., "Impact Driven Supply of Sodium and Potassium to the Atmosphere of Mercury", to appear in ICARUS, 1988.

NASA SP-8013, "NASA Space Vehicle Design Criteria (Environment); Meteoroid Environment Model - 1969 [Near Earth to Lunar Surface]", 1969.

NASA SP-8038, "NASA Space Vehicle Design Criteria (Environment); Meteoroid Environment Model - 1970 [Interplanetary and Planetary]", 1970.

NASA SP-8042, "NASA Space Vehicle Design Criteria (Structures); Meteoroid", 1970.

Rawer, K. (Chairman), "International Reference Ionosphere--IRI 79 (edited by J.V. Lincoln and R.O. Conkright), World Data Center A, Rpt. UAG-82, Nov., 1981

Rawer, K., and P.A. Bradley, editors, "International Reference Ionosphere-Status 1986/87", The Committee on Space Research, Pergamon Press, New York, 1987.

Reagan, J.B., W.L. Imhof, and V.F. Moughan, "Characteristics of the August 1972 Solar Particle Events as Observed over the Earth's Polar Caps", in Collected Data Reports on August 1972 Solar-Terrestrial Events, Report UAS-28, Part III, World Data Center A for Solar-Terrestrial Physics, Boulder, CO., p. 676, July, 1973.

Sawyer, D.M., and J.J. Vette, "AP8 Trapped Proton Environment for Solar Maximum and Solar Minimum", NSSDC 76-06, NASA-GSFC, 1976.

Slowey, J.W., "Dynamic Model of the Earth's Upper Atmosphere", NASA Contractor Report 3835, Sept., 1984.

Tsao, C.H., R. Silberberg, J.H. Adams, and J.R. Letaw, "Cosmic Ray Effects on Microelectronics, Part III: Propagation of Cosmic Rays in the Atmosphere", NRL Memorandum Report 5402, Naval Research Laboratory, Washington, DC 20375, 1984.

Vampola, A., "Solar Cycle Effects on Trapped Energetic Particles", to appear in J. SPACECRAFT, 1989.

Vette, J.I., et al., "AE8 Model for Inner and Outer Zone Electrons at Solar Minimum and Solar Maximum: Unpublished electron model replacing AE5, AE6, and AEI7" (see NSSDC reports 72-06, 72-13 (AE-4), 72-10 (AE5), and 76-04 (AE6), 1986.

Whitten, R.C., and I.G. Poppoff, "Fundamentals of Aeronomy", J. Wiley & Sons, Inc., New York, 1971.

FIGURE CAPTIONS

1. Neutral atmosphere vertical density profile in units of $n^{\#}/cm^{-3}$ (adapted from Carrigan and Skrivanek [1974]).

2. Polar view of the northern hemisphere. Polar coordinates are employed such that the radial distance is in intervals of equal latitude (0° is the equator) while the angular coordinate is east longitude. Neutral atmosphere conditions for K_p=6, $F_{10.7}$=220, Day No#=357.5, and height=400 km as computed by the Jacchia 1972 model are shown.

3. Neutral temperature for the Jacchia 1972 model in K (same conditions as Fig. 2).

4. Number density of Oxygen for the Jacchia 1972 model in $no^{\#}/cm^{-3}$ (same conditions as Fig. 2).

5. Northern hemisphere view of percentage deviation of neutral density (N_2) and temperature from the Jacchia 1972 model for a geomagnetic storm of K_p=6$_0$ (after Slowey [1984]). "ST" means storm conditions; "QT" means normal Jacchia 1972 prediction.

6. Meridional cross section of the Earth's magnetosphere showing the dominate plasma regions and the magnetic field configuration for a noon-midnight cut.

7. Polar view of the northern hemisphere at 400 km as in Fig. 2 for the total magnetic field amplitude as predicted by the POGO magnetic field model. Units are G.

8. Polar view of the northern hemisphere as in Fig. 2 for the absolute vxB induced electric field at 400 km. The POGO magnetic field and a 90° orbital inclination were assumed.

9. Solar photon flux density spectrum at the Earth (after Grard [1973]).

10. The Zurich smoothed sunspot number variation between 1950 and 1988. Superimposed on the figure are the fluences for the individual large solar flare proton events during the same period (from Daly [1988]).

11. Structure of the Solar Wind magnetic field background and that associated with a high speed solar stream showing the effects of compression and shock. Also shown is the hypothesized termination shape for the Solar Wind beyond the orbit of Pluto.

12. Representative midlatitutde daytime and nightime electron density profiles (top) and temperature profiles (bottom) for sunspot maximum (———) and sunspot minimum (-------); Carrigan and Skrivanek [1974].

13. Representative midlatitutde daytime and nightime ion composition profiles for daytime (top) and nighttime (bottom) for sunspot minimum; Carrigan and Skrivanek [1974].

14. Northern hemisphere view (coordinates as in Fig. 2) of the electron environment at 400 km for a sunspot number of 100 as predicted by the IRI model. a) electron density; b) electron temperature.

15. Representative differential electron flux spectrum for an auroral arc (Gussenhoven et al. [1985]).

16. Constant flux contours (after Daly [1988]) for protons and electrons as predicted by the AE8/AP8 radiation models (Vette et al. [1986]; Sawyer and Vette [1976]).

17. Comparison between relative abundances of the elements from hydrogen to the iron group normalized to carbon (C=100) for Cosmic Rays (heavy line) and for the Solar System (light line). From Meyer et al. [1974].

18. The energy spectra of Cosmic Ray protons (line) and electrons (points) as measured near the Earth. From Meyer et al. [1974].

19. Comparison of the August 1972 solar flare proton event fluxes with the Galactic Cosmic Ray fluxes for 1972 (Reagan et al. [1973]).

20. Comparison between the predicted debris flux from Kessler et al. [1989] and the natural meteoroid flux from NASA SP8013 at 500 km.

21. Cometary meteor velocity distribution as measured by different groups at 1 AU (from Morgan et al. [1988]).

22. Debris flux as a function of altitude as measured by the U.S. Space Command and as predicted by the debris model (Kessler et al. [1989]) for 10 cm objects in January 1987. An orbital inclination of 60° is assumed. From Kessler et al. [1989].

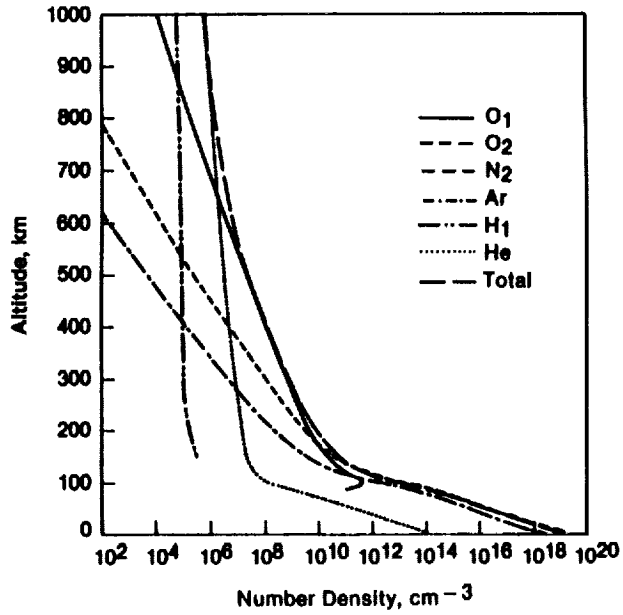

FIGURE 1.

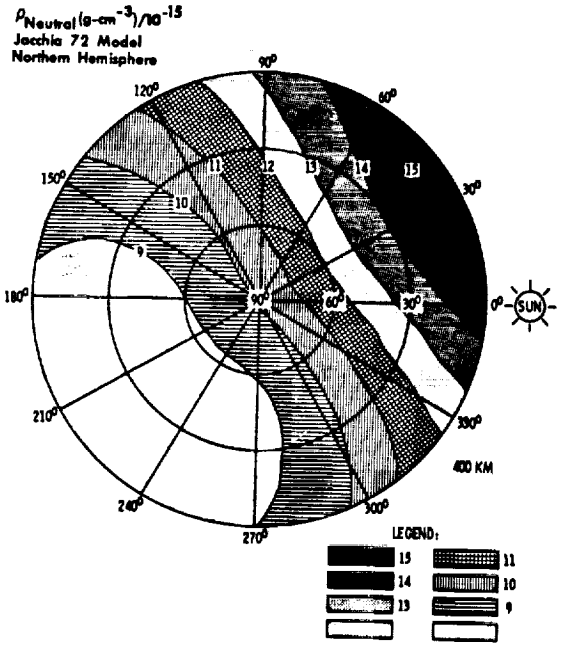

FIGURE 2

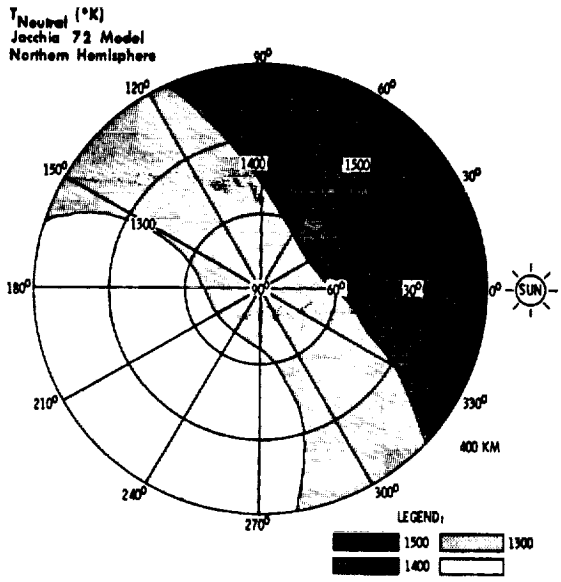

FIGURE 3.

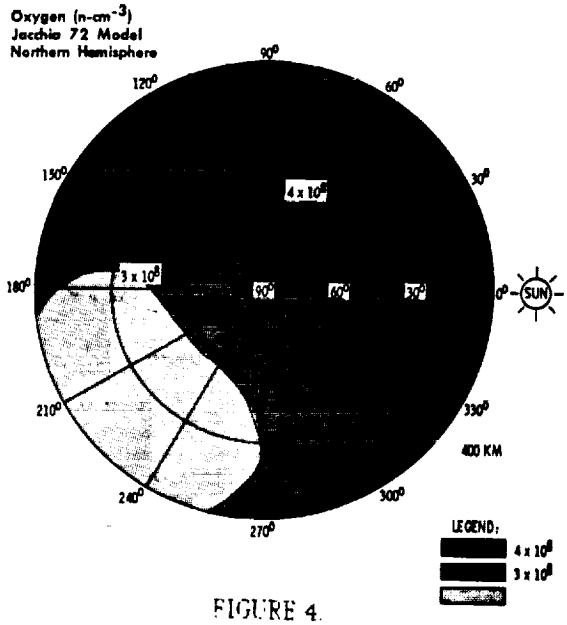

FIGURE 4.

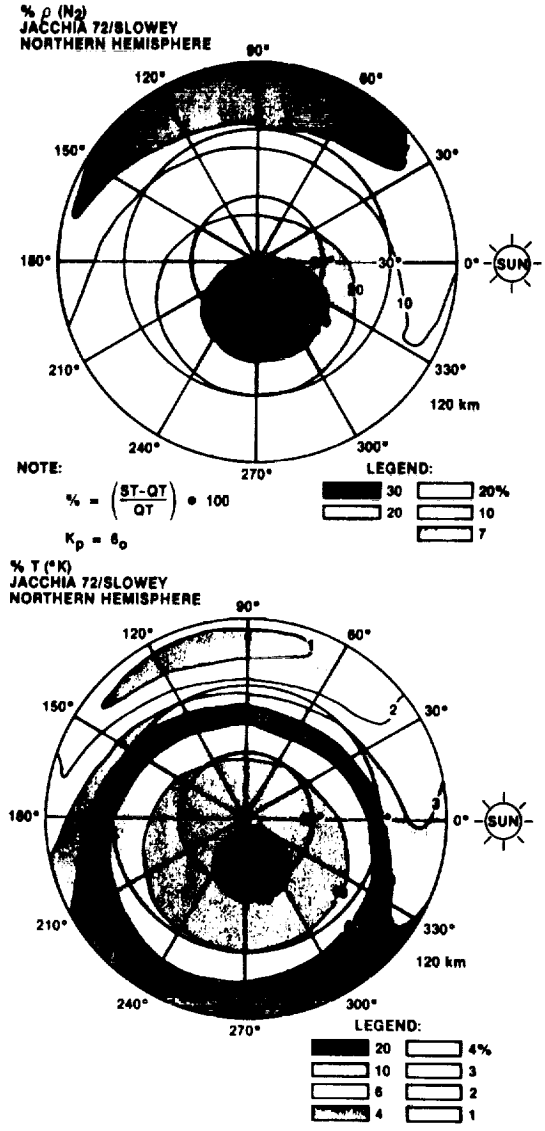

FIGURE 5.

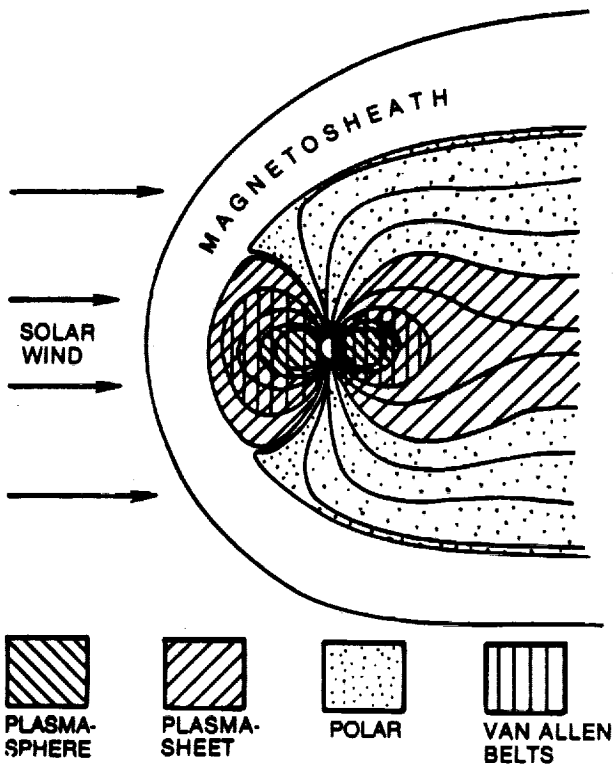

FIGURE 6.

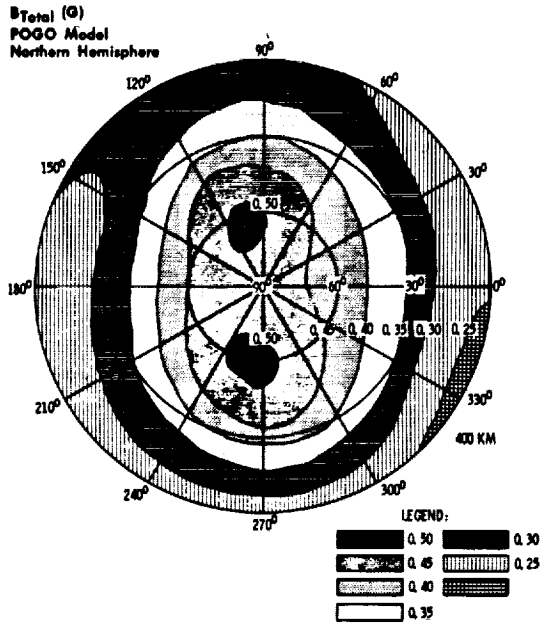

FIGURE 7

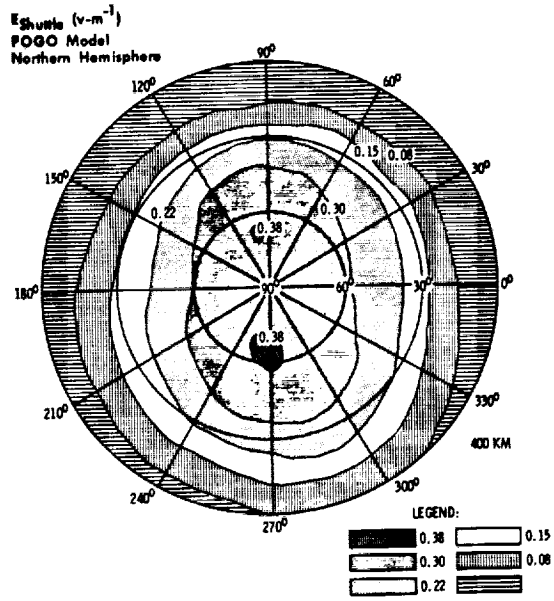

FIGURE 8.

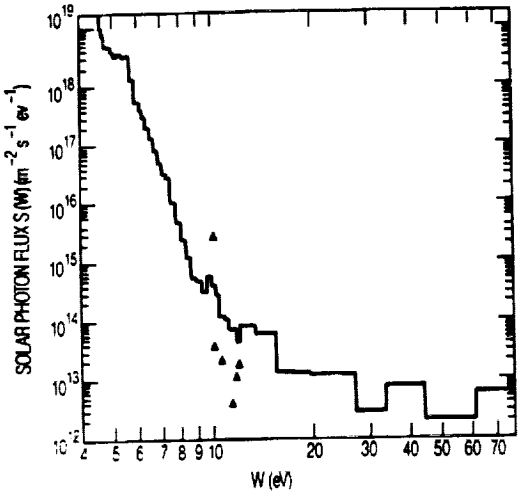

FIGURE 9

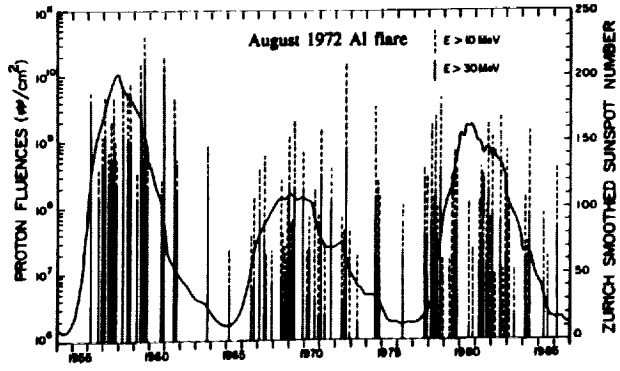

FIGURE 10.

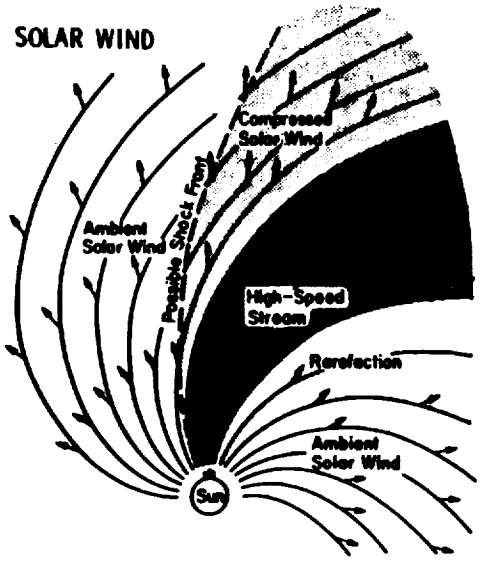

MAGNETIC HELIOSPHERE

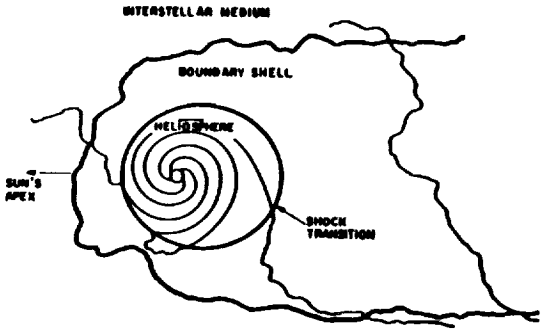

FIGURE 11.

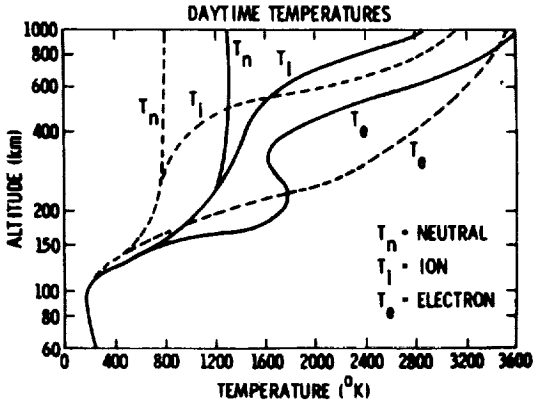

FIGURE 12A.

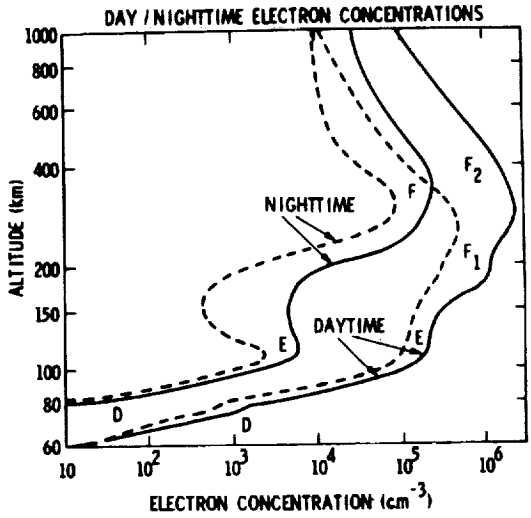

FIGURE 12B

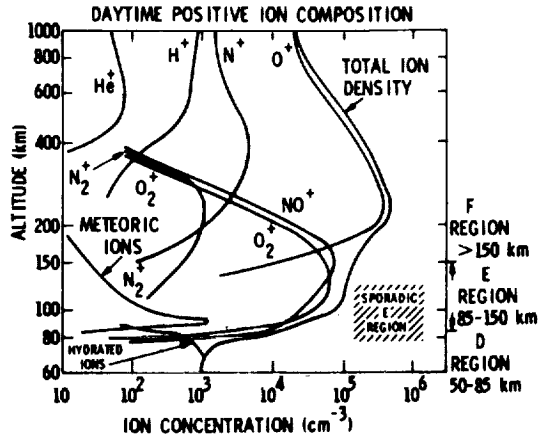

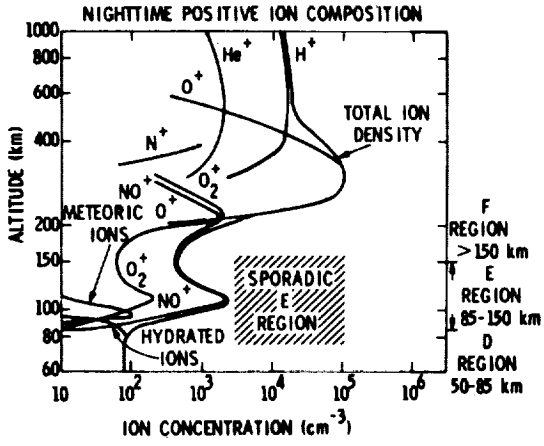

FIGURE 13

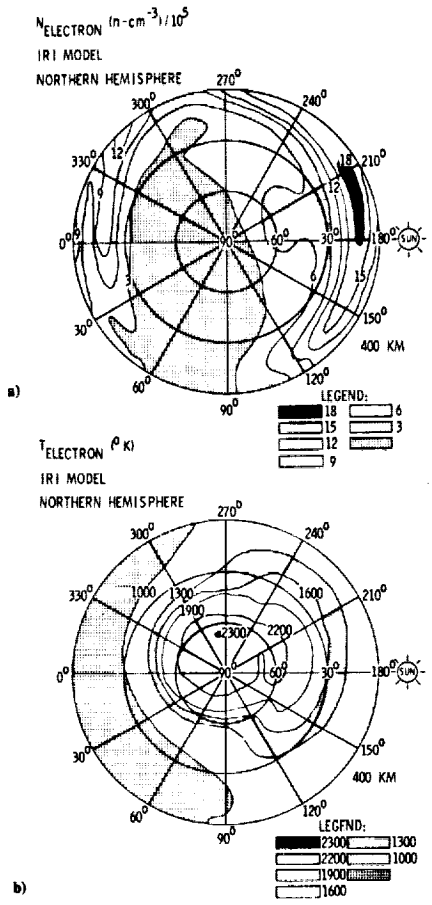

FIGURE 14

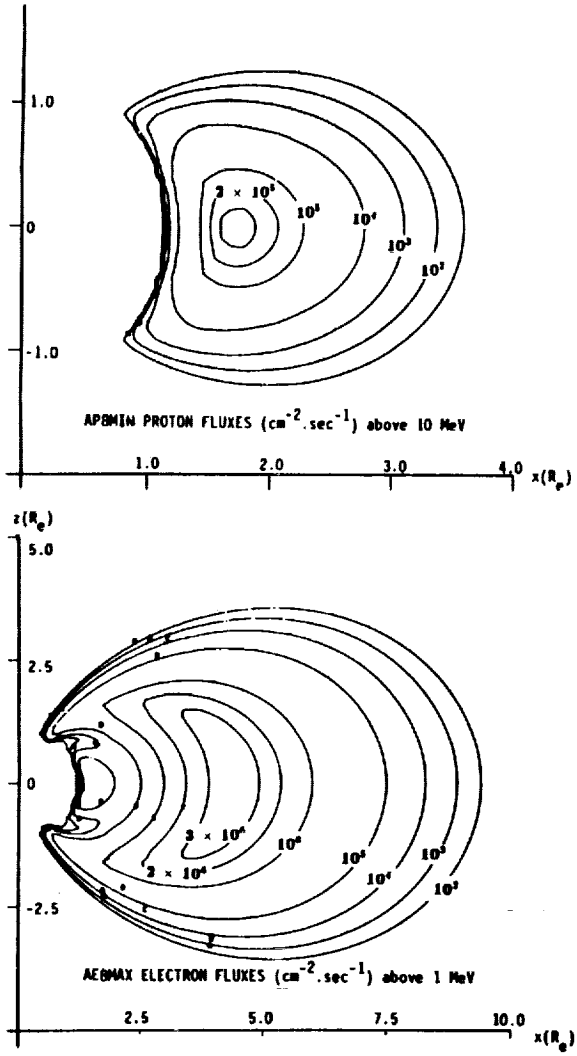

FIGURE 16

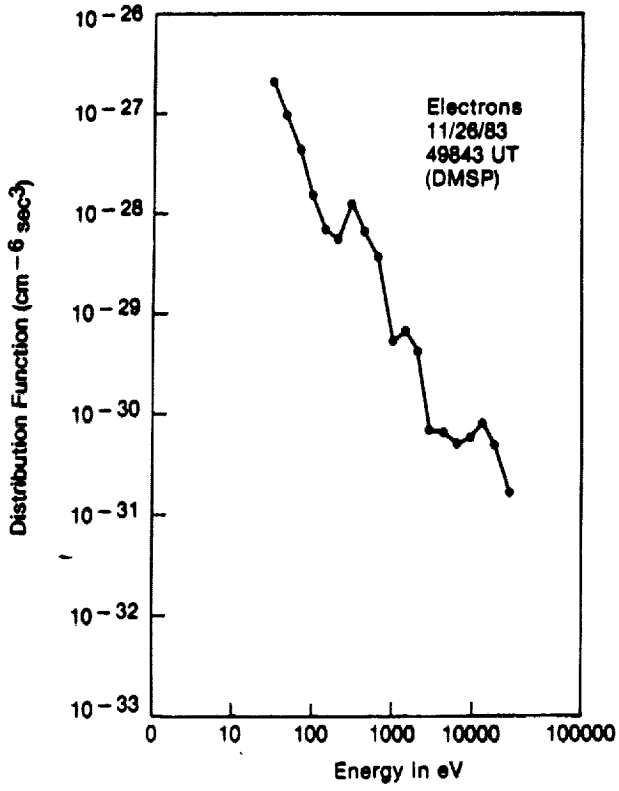

FIGURE 15.

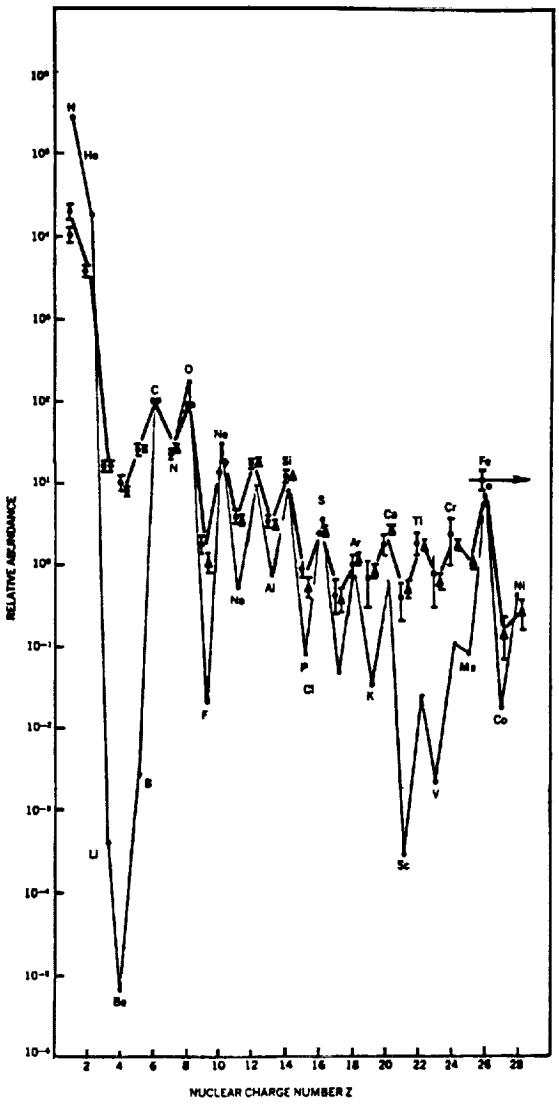

FIGURE 17

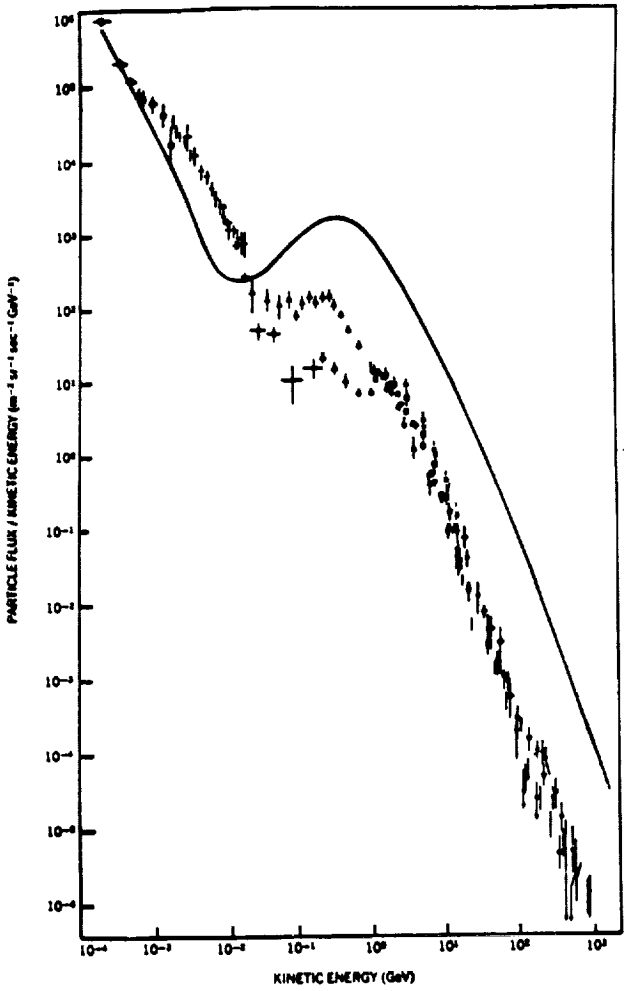

FIGURE 18

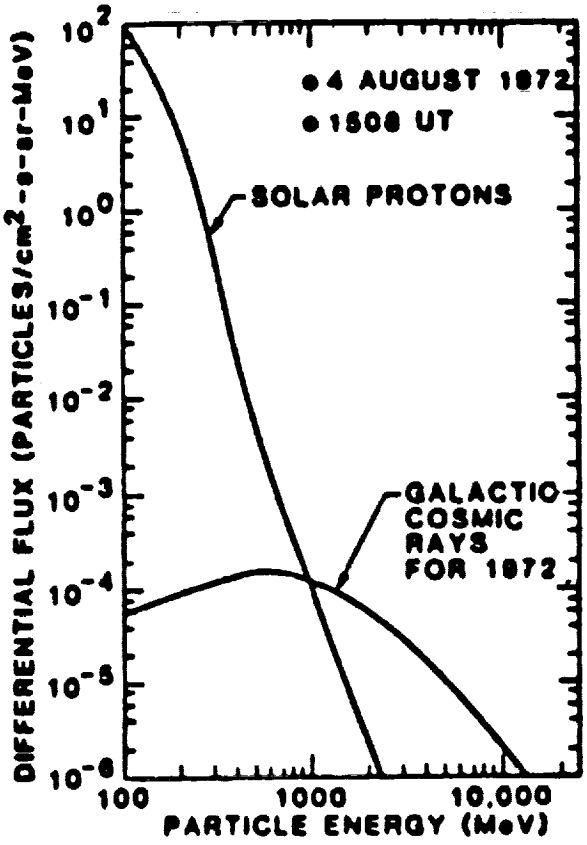

FIGURE 19

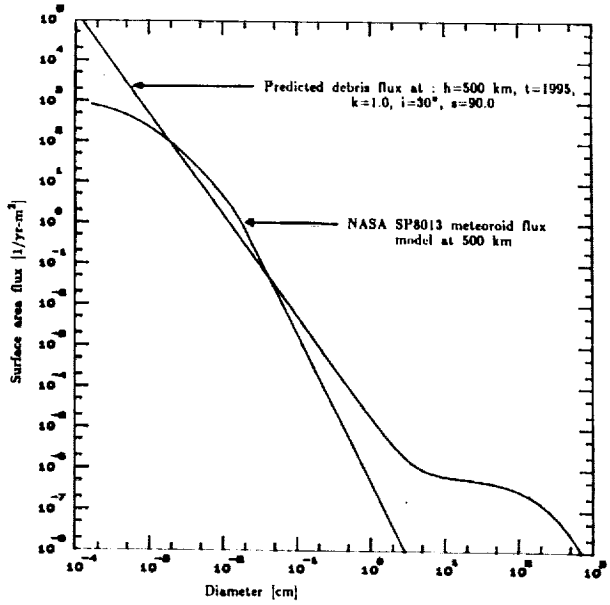

FIGURE 20

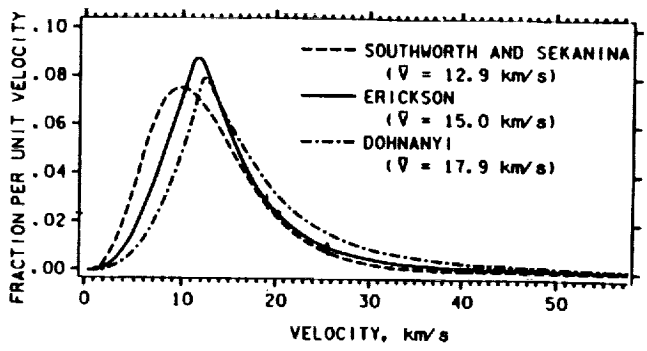

FIGURE 21

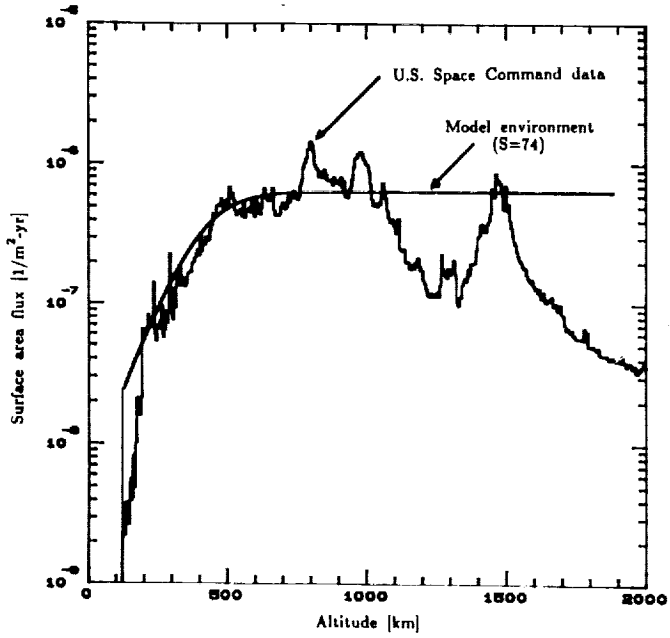

FIGURE 22